European Radiology (2023) 33:1364–1377
https://doi.org/10.1007/s00330-022-09105-7

GASTROINTESTINAL

Comparison of imaging findings of macrotrabecular-massive hepatocellular carcinoma using CT and gadoxetic acid–enhanced MRI

Hyunho Cha[1] · Jin-Young Choi[1] · Young Nyun Park[2] · Kyunghwa Han[3] · Mi Jang[4] · Myeong-Jin Kim[1] · Mi-Suk Park[1] · Hyungjin Rhee[1]

Received: 17 June 2022 / Revised: 17 June 2022 / Accepted: 9 August 2022 / Published online: 24 August 2022

Abstract

Objectives To investigate the imaging findings of macrotrabecular-massive hepatocellular carcinoma (MTM-HCC) on CT and MRI, and examine their diagnostic performance and prognostic significance.

Methods We retrospectively enrolled 220 consecutive patients who underwent hepatic resection between June 2009 and December 2013 for single treatment–naïve HCC, who have preoperative CT and gadoxetic acid–enhanced MRI. Independent reviews of histopathology and imaging were performed by two reviewers. Previously reported imaging findings, LI-RADS category, and CT attenuation of MTM-HCC were investigated. The diagnostic performance of the MTM-HCC diagnostic criteria was compared across imaging modalities.

Results MTM-HCC was associated with ≥ 50% arterial phase hypovascular component, intratumoral artery, arterial phase peritumoral enhancement, and non-smooth tumor margin on CT and MRI ($p < .05$). Arterial phase hypovascular components were less commonly observed on MRI subtraction images than on CT or MRI, while non-rim arterial phase hyperenhancement and LR-5 were more commonly observed on MRI subtraction images than on MRI ($p < .05$). MTM-HCC showed lower tumor attenuation in the CT arterial phase ($p = .01$). Rhee's criteria, defined as ≥ 50% hypovascular component and ≥ 2 ancillary findings (intratumoral artery, arterial phase peritumoral enhancement, and non-smooth tumor margin), showed similar diagnostic performance for MRI (sensitivity, 41%; specificity, 97%) and CT (sensitivity, 31%; specificity, 94%). Rhee's criteria on CT were independent prognostic factors for overall survival.

Conclusion The MRI diagnostic criteria for MTM-HCC are applicable on CT, showing similar diagnostic performance and prognostic significance. For MTM-HCC, arterial phase subtraction images can aid in the HCC diagnosis by depicting subtle arterial hypervascularity.

Key points

- *MTM-HCC on CT demonstrated previously described MRI findings, including arterial phase hypovascular component, intratumoral artery, arterial phase peritumoral enhancement, and necrosis.*
- *The MRI diagnostic criteria for MTM-HCC were also applicable to CT, showing comparable diagnostic performance and prognostic significance.*
- *On arterial phase subtraction imaging, MTM-HCC more frequently demonstrated non-rim enhancement and LR-5 and less frequently LR-M than MRI arterial phase, which may aid in the diagnosis of HCC.*

Keywords Carcinoma, hepatocellular · Liver neoplasm · Gadoxetic acid · Magnetic resonance imaging · Computed tomography

✉ Hyungjin Rhee
hjinrhee@yuhs.ac

[1] Department of Radiology, Research Institute of Radiological Science, Severance Hospital, Yonsei University College of Medicine, 50-1 Yonsei-Ro, Seodaemun-gu, Seoul 03722, South Korea

[2] Department of Pathology, Graduate School of Medical Science, Brain Korea 21 Project, Yonsei University College of Medicine, Seoul, South Korea

[3] Department of Radiology, Research Institute of Radiological Science, Center for Clinical Imaging Data Science, Yonsei University College of Medicine, Seoul, South Korea

[4] Department of Pathology, National Health Insurance Service Ilsan Hospital, Goyang, South Korea

Abbreviations

APHE	Arterial phase hyperenhancement
CT	Computed tomography
ER	Early recurrence
HCC	Hepatocellular carcinoma
LI-RADS	Liver Imaging Reporting and Data System
MRI	Magnetic resonance imaging
MTM-HCC	Macrotrabecular-massive hepatocellular carcinoma
OS	Overall survival
ROI	Region of interest

Introduction

Macrotrabecular-massive hepatocellular carcinoma (MTM-HCC), a recently proposed histological subtype of HCC, has been highlighted because of its peculiar transcriptomic and genetic characteristics and poor prognosis after curative treatment [1–5].

Several imaging diagnostic criteria for MTM-HCC have been proposed. One report proposed a combination of arterial phase hypovascularity and imaging features related to microvascular invasion, including intratumoral artery, arterial phase peritumoral enhancement, and non-smooth tumor margin, and it could provide a sensitivity of 46–47% with a specificity of 94–96% [6]. Another report proposed the combination of absence of enhancement and T2 hyperintensity, namely "substantial necrosis", which represents the necrotic tumor area. Substantial necrosis reportedly has a sensitivity of 65% and a specificity of 93% [7]. Both diagnostic criteria for MTM-HCC are based on the presence of an intratumoral hypovascular area, reflecting the hypoxic microenvironment of MTM-HCC. MTM-HCC has lower microvascular density, a larger area of tumor necrosis, and higher expression of hypoxia-related genes such as *CA9*, *EPO*, and *VEGFA* compared to non-MTM-HCC [8, 9]. Although hypovascularity is a clue to MTM-HCC, it may also act as an obstacle to an HCC imaging diagnosis. The arterial phase subtraction image on MRI depicts the subtle arterial enhancement of the tumor and may aid in HCC diagnosis [10]. However, the imaging findings of MTM-HCC on arterial subtraction imaging and their potential implication on HCC diagnosis have not been investigated.

Previously reported MRI criteria of MTM-HCC were associated with poor outcomes following hepatic resection; thus, they might be useful for clinical decision-making prior to treatment [6, 7]. However, MRI is not always used in HCC patients because of its limited availability and high cost, which is even more critical in the clinical setting within developing countries [11]. MRI also requires a long scan time with multiple breath-holds and might not be feasible in patients with a poor general condition. Computed tomography (CT) is a more appropriate diagnostic tool in these situations. To our knowledge, however, few publications have described CT findings of MTM-HCC, and no study has comprehensively compared the diagnostic performance of various imaging criteria on CT [12].

Therefore, this study aimed to investigate the imaging findings of MTM-HCC on CT and MRI, including arterial phase subtraction images, and examine their diagnostic performance and prognostic significance.

Materials and methods

Subject

This retrospective study was conducted in accordance with the ethical guidelines of the Declaration of Helsinki and approved by the Institutional Review Board of Severance Hospital, Seoul, Korea, which waived the requirement for patient consent (4-2021-0965). We enrolled consecutive patients with pathologically confirmed HCC after hepatic resection at Severance Hospital between June 2009 and December 2013. We excluded patients who received any treatment prior to surgery, who had multiple HCC, for whom gadoxetic acid–enhanced MRI including arterial phase subtraction imaging or liver dynamic CT within 3 months before surgery was unavailable, and for whom pathology slides were not available for review. When there was a small (< 1 cm) satellite lesion in the same segment, the case was considered a single HCC and not excluded from the study. Cases in which intraoperative radiofrequency ablation was performed on hepatic lesion(s) were considered multiple HCC and excluded. Finally, 220 patients with 220 HCC were included in this study (Fig. 1).

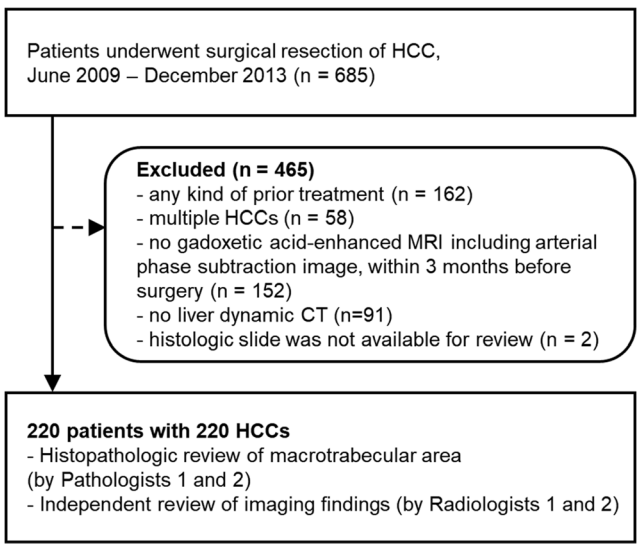

Fig. 1 Flow diagram of the patient enrolment process. CT, computed tomography; HCC, hepatocellular carcinoma; MRI, magnetic resonance imaging

All of 220 patients overlapped with our previous study [6]; in fact, 88 patients (40%) and 132 patients (60%) overlapped with the training and validation sets of the previous study. The prior study dealt with MRI findings of MTM-HCC, whereas in this manuscript we investigated CT findings of MTM-HCC in comparison with MRI findings.

Histopathologic data

Histopathologic data including tumor size, differentiation (Edmondson-Steiner grade), capsule formation, microvascular invasion, satellite nodules, and tumor necrosis were retrospectively collected from the pathology reports. Two pathologists (Y.N.P. and M.J.) independently reviewed the hematoxylin-eosin-stained slides to determine whether they corresponded to MTM-HCC. MTM-HCC was defined as HCC with a predominant (≥ 50%) macrotrabecular pattern characterized by trabeculae more than six cells thick [2]. After a 1-month independent review, two pathologists met to draw consensus data, which were used as reference standards for imaging diagnosis.

Gadoxetic acid–enhanced MRI and dynamic CT

All gadoxetic acid–enhanced MRI and dynamic CT images evaluated in our study met the technical acquisition standards of LI-RADS version 2018.

Please refer to Supplementary Material and Methods and Supplementary Tables 1 and 2 for imaging protocols, clinical and lab data, and measurement of outcome.

Image analysis

Two radiologists (H.R. and H.C.), who had 9 and 2 years of experience in interpreting liver dynamic images, independently reviewed the CT and MRI images using a picture archiving and communication system (Centricity; GE Healthcare). Two radiologists reviewed the dynamic CT first, reviewed the MRI after approximately 1 month, and then met to create consensus data. The arterial phase hypovascular component (< 20%, 20–49%, or ≥ 50% tumor volume) was defined as an arterial phase hypovascular tumor area combined with peripheral or spot-like hypervascular foci [6]; intratumoral artery as discrete arteries within the tumor on the arterial phase images [13]; arterial phase peritumoral enhancement as the detectable portion of a crescent- or polygon-shaped enhancement outside the tumor margin with broad contact with the tumor border in the arterial phase becoming isointense with background liver parenchyma in the delayed phase [14]; and a non-smooth tumor margin as an irregular tumor margin with a budding portion at its periphery protruding into the liver parenchyma [14] observed on the hepatobiliary phase of MRI or portal phase of CT. On MRI, tumor necrosis was defined as a tumor area with bright T2 signal intensity [7] subclassified into three categories, central, stippled, and linear necrosis. Central necrosis was defined as conglomerated necrosis of the tumor center, stippled necrosis as multiple separate point-shaped foci of necrosis, and linear necrosis as linear and/or branching necrosis. On CT images, we evaluated necrosis or severe ischemia based on the definition of LI-RADS version 2018 [15]. Additionally, in CT and MRI, we assessed non-rim arterial phase hyperenhancement (APHE) and blood product in mass as defined by LI-RADS. The LI-RADS category was determined using CT and MRI, taking into account all major and ancillary features. The proportions of arterial phase hypovascular component, non-rim APHE, and LI-RADS categories were additionally reviewed using subtraction images of the arterial phase from pre-contrast MRI images.

Using the reviewed imaging findings, we determined whether each HCC meets the previously reported imaging criteria for MTM-HCC on CT and MRI. The imaging criteria were defined follows: (1) Rhee's criteria, arterial hypovascular component (≥ 50%) with two or more of intratumoral artery, arterial phase peritumoral enhancement, and non-smooth tumor margin [6]; (2) modified Mule's criteria, arterial phase hypovascular component (≥ 50%) with stippled necrosis on MRI, and arterial phase hypovascular component (≥ 50%) with necrosis/severe ischemia on CT [7]; and (3) Feng's criteria, the presence of necrosis/severe ischemia or blood product [12].

Quantitative analysis

One radiologist (H.C.) measured the attenuation of the HCC and non-tumor liver in each phase of the CT images. For the measurement of HCC, a circular region of interest (ROI) was made at the maximal positions in the HCC and measured at the same position in each dynamic phase. The attenuation of the non-tumor liver was measured at the contralateral lobe of the liver, excluding the portions around the blood vessels, gallbladder bed, arterioportal shunt, and subcapsular area of the liver. The ROI for the non-tumor liver was made to be 200–300 mm^2 in a circle.

Statistical analysis

Inter-reader agreement is expressed using Cohen's kappa coefficient. A kappa statistic of 0.8–1.0, 0.6–0.79, 0.40–0.59, 0.2–0.39, and 0–0.19 was considered excellent, good, moderate, fair, and poor agreement, respectively. To compare clinicopathologic characteristics and imaging features, we used a Mann–Whitney *U* test for continuous variables and a chi-

square or Fisher's exact test for categorical variables. The positive rate, sensitivity, and specificity of the imaging findings or diagnostic criteria were compared using the McNemar test. Survival analyses were performed using the Kaplan–Meier method, log-rank test, and Cox regression analysis. The statistical analyses were performed using R software (version 4.1.1; https://www.R-project.org/). Statistical significance was defined as a two-sided p value < .05.

Results

Clinicopathologic findings of MTM-HCC

The clinicopathological characteristics of the study population are summarized in Table 1. Of the 220 patients with single HCC (median age, 55 years; interquartile range [IQR], 51–63 years; 173 men and 47 women), 39 (18%) had MTM-HCC. MTM-HCC was associated with high serum AFP (p < .001) and PIVKA-II (p < .001), larger tumor size (p = .01), poorer

Table 1 Patients' clinicopathologic characteristics

Clinicopathologic features	Available data (*n*)	*n* (%) or median (interquartile range)
Clinical features		
Age (year)	220	55 (51–63)
Sex (male/female)	220	173 (79%)/47 (21%)
Etiology	220	
Hepatitis B		191 (87%)
Hepatitis C		5 (2%)
Alcohol		12 (6%)
Unknown		12 (6%)
Cirrhosis	220	121 (55%)
High-risk for HCC (LI-RADS v2018)	220	202 (92%)
Child-Pugh class (A/B)	220	219 (100%)/1 (1%)
BCLC stage (0/A)	220	36 (16%)/184 (84%)
Aspartate transaminase (IU/L)	220	29 (23–41)
Alanine transaminase (IU/L)	220	30 (23–44)
Albumin (g/dL)	220	4.3 (4.1–4.6)
Platelet (1000/μL)	220	160 (128–212)
Total bilirubin (mg/dL)	220	0.7 (0.6–0.9)
PT/INR	220	1.0 (0.9–1.0)
Alpha-fetoprotein (ng/mL)	219	18.5 (3.9–219.5)
PIVKA-II (mAU/mL)	219	760. (29.5–355.5)
Tumor pathology		
Tumor size (cm)	220	3.0 (2.2–4.5)
Differentiation (Edmondson-Steiner grade)	220	
I		12 (6%)
II		168 (76%)
III or IV		40 (18%)
Capsule formation	220	
Absent		37 (17%)
Partial		116 (53%)
Complete		67 (31%)
Microvascular invasion	220	98 (45%)
Satellite nodule	220	10 (5%)
Necrosis (≥ 5%)	220	50 (23%)
Hemorrhage (≥ 5%)	220	82 (37%)
Macrotrabecular-massive HCC	220	39 (18%)

BCLC, Barcelona Clinic Liver Cancer; *HCC*, hepatocellular carcinoma; *INR*, international normalized ratio; *LI-RADS*, Liver Imaging Reporting and Data System; *PIVKA-II*, protein induced by vitamin K absence or antagonist-II; *PT*, prothrombin time

Table 2 Imaging features of macrotrabecular-massive hepatocellular carcinoma (MTM-HCC) versus non-MTM-HCC

Imaging findings	MRI			MRI, using arterial phase subtraction			CT		
	Non-MTM-HCC (n = 181, 82%)	MTM-HCC (n = 39, 18%)	p value	Non-MTM-HCC (n = 181, 82%)	MTM-HCC (n = 39, 18%)	p value	Non-MTM-HCC (n = 181, 82%)	MTM-HCC (n = 39, 18%)	p value
Arterial phase hypovascular component			< .001*			< .001*			< .001*
< 20%	109 (60%)	3 (8%)		129 (71%)	16 (41%)		111 (61%)	8 (21%)	
20–49%	54 (30%)	10 (26%)		45 (25%)	8 (21%)		44 (24%)	6 (15%)	
50–100%	18 (10%)	26 (67%)		7 (4%)	15 (39%)		26 (15%)	25 (64%)	
Intratumoral artery	30 (17%)	18 (46%)	< .001*				33 (18%)	16 (41%)	.004*
Arterial phase peritumoral enhancement	27 (15%)	20 (51%)	< .001*				20 (11%)	10 (26%)	.03*
Non-smooth tumor margin	82 (45%)	28 (72%)	.01*				62 (34%)	24 (62%)	.003*
Necrosis, central (MRI)	17 (9%)	4 (10%)	.77						
Necrosis, stippled (MRI)	37 (20%)	19 (49%)	.001*						
Necrosis, linear (MRI)	8 (4%)	2 (5%)	.69						
Necrosis or severe ischemia (CT)							62 (34%)	28 (72%)	< .001*
Blood product	29 (16%)	12 (31%)	.06				7 (4%)	2 (5%)	.66
Non-rim APHE	163 (90%)	25 (64%)	< .001*	171 (95%)	32 (82%)	.02*	157 (87%)	27 (69%)	.02*
LI-RADS category†			.002*			.03*			.002*
LR-TIV	0 (0%)	1 (3%)		0 (0%)	1 (3%)		0 (0%)	2 (6%)	
LR-M	13 (8%)	9 (27%)		9 (5%)	5 (15%)		14 (8%)	8 (24%)	
LR-3	0 (0%)	0 (0%)		0 (0%)	0 (0%)		5 (3%)	1 (3%)	
LR-4	22 (13%)	4 (12%)		20 (12%)	2 (6%)		9 (5%)	3 (9%)	
LR-5	133 (79%)	20 (59%)		139 (83%)	26 (76%)		140 (83%)	20 (59%)	

Unless otherwise indicated, data represent number of hepatocellular carcinomas with percentage in parentheses

*Statistically significant results from chi-square or Fisher's exact test

† Categorization was performed in high-risk patients for HCC defined by LI-RADS version 2018

APHE, arterial phase hyperenhancement; *CT*, computed tomography; *LI-RADS*, Liver Imaging Reporting and Data System; *MRI*, magnetic resonance imaging; *MTM-HCC*, macrotrabecular-massive hepatocellular carcinoma

Non-smooth tumor margin was assessed in MRI using hepatobiliary phase and in CT using portal phase

differentiation (p = .001), more frequent microvascular invasion (p < .001), and tumor necrosis (≥ 5%) (p = .001) (Supplementary Table 3). Intratumoral hemorrhage was not significantly associated with MTM-HCC (p = .07).

MRI and CT features of MTM-HCC

The imaging findings of MTM-HCC are summarized in Table 2, and the inter-reader agreement of pathologic and

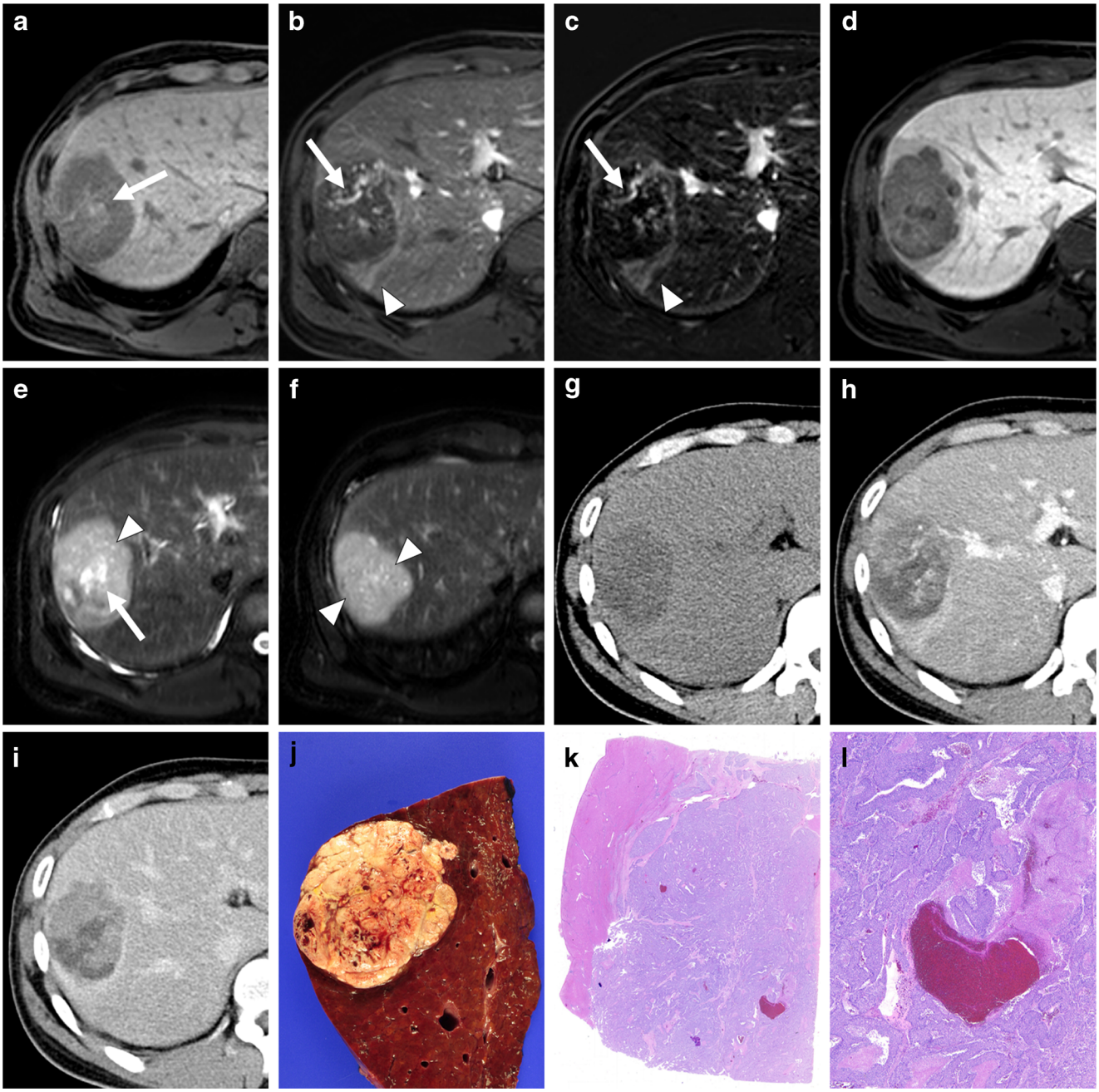

Fig. 2 A 29-year-old man with hepatitis B virus–related cirrhosis and macrotrabecular-massive hepatocellular carcinoma (MTM-HCC). Gadoxetic acid–enhanced magnetic resonance imaging (MRI) demonstrated an approximately 7.5-cm HCC in segment 8. The lesion showed blood product (arrow) on a pre-contrast T1-weighted image (**a**), ≥ 50% hypovascular component with intratumoral artery (arrows), arterial phase peritumoral enhancement (arrowheads) in arterial phase images (**b**) and arterial phase subtraction image (**c**), non-smooth tumor margin in the hepatobiliary phase (**d**), and both central (arrow) and stippled necrosis (arrowheads) on a T2-weight image (**e** and **f**). CT also demonstrated the absence of blood product in the pre-contrast image (**g**), a ≥ 50% hypovascular component, intratumoral artery, and arterial phase peritumoral enhancement in the arterial phase (**h**), a non-smooth tumor margin, and necrosis or severe ischemia in the portal phase (**h** and **i**). Rhee's and modified Mule's criteria were positive on CT and MRI, and Feng's CT criteria were also positive. The lesion was MTM-HCC and exhibited multifocal hemorrhagic necrotic foci in the gross specimen (**j**) and hematoxylin-eosin staining (original magnification, scan view (**k**), × 20 (l)). Intrahepatic metastasis occurred 3 months after a right lobectomy, and the patient died 8 months post-surgery

imaging findings is listed in Supplementary Table 4. On MRI, MTM-HCC demonstrated more frequent arterial phase hypovascular component ($p < .001$), intratumoral artery ($p < .001$), arterial phase peritumoral enhancement ($p < .001$), non-smooth tumor margin ($p = .01$), and stippled necrosis ($p = .001$) than non-MTM-HCC. Central necrosis, linear necrosis, and blood products were not associated with MTM-HCC. MTM-HCC less frequently showed non-rim APHE ($p < .001$), and significantly different LI-RADS categories ($p = .002$; more frequent LR-M and less frequent LR-5). On the arterial phase subtraction image, MTM-HCC more frequently demonstrated the arterial phase hypovascular component ($p < .001$), less frequently demonstrated the non-rim APHE ($p = .02$), and showed significantly different patterns of LI-RADS categories ($p = .03$).

On the CT, MTM-HCC also more frequently demonstrated the arterial phase hypovascular component ($p < .001$), intratumoral artery ($p = .004$), arterial phase peritumoral enhancement ($p = .03$), non-smooth tumor margin ($p = .003$), and necrosis or severe ischemia ($p < .001$), less frequently demonstrated non-rim APHE ($p = .02$), and showed significantly different LI-RADS categories ($p = .002$) compared with non-MTM-HCC (Fig. 2). In the quantitative analysis of CT attenuation (Fig. 3; Supplementary Table 5), the tumor attenuations of MTM-HCC were significantly lower than those of non-MTM-HCC in the arterial and portal phases ($p = .01$ and $p = .002$, respectively). The difference between tumor and liver attenuation was also compared; [tumor attenuation − liver attenuation] was significantly lower in the MTM-HCC in the pre-contrast, arterial, portal, and delayed phases ($p = .01$, $p < .001$, $p < .001$, and $p = .01$, respectively).

Differences in imaging features of MTM-HCC between imaging modalities

MTM-HCC less frequently showed the arterial phase hypovascular component (≥ 20% and ≥ 50%) in the MRI arterial subtraction image than in the arterial phase on MRI ($p < .001$ and $p < .001$, respectively) and CT ($p = .03$ and $p = .02$, respectively) (Table 3). MTM-HCC more frequently showed non-rim APHE ($p = .01$) and LR-5 ($p = .02$) and less frequently showed LR-M ($p = .03$) in the MRI arterial subtraction image than in the MRI arterial phase image (Fig. 4). A similar tendency was observed for non-MTM-HCC.

Differences in diagnostic performance between MRI and CT criteria for MTM-HCC

The diagnostic performance of each imaging feature and diagnostic criterion is listed in Table 4. A hypovascular component ≥ 20% on MRI showed a high negative predictive value (NPV) of 97%. On CT, the ≥ 20% hypovascular component also showed a high NPV of 93%, which was not significantly different from that on MRI ($p = .06$).

Rhee's criteria were defined by a hypovascular component (≥ 50%) with two or more intratumoral arteries, arterial phase peritumoral enhancement, and non-smooth tumor margin. The sensitivity and specificity of Rhee's criteria on MRI were 41% and 97%, respectively. Rhee's criteria on MRI were used as a reference for diagnostic performance, as it is the only criterion validated in a multicenter study. Since only the stippled pattern of necrosis was significantly associated with MTM-HCC and the proportion of necrotic/ischemic tumor area was not easy to determine, we modified Mule's criteria as follows: hypovascular component (≥ 50%) with stippled

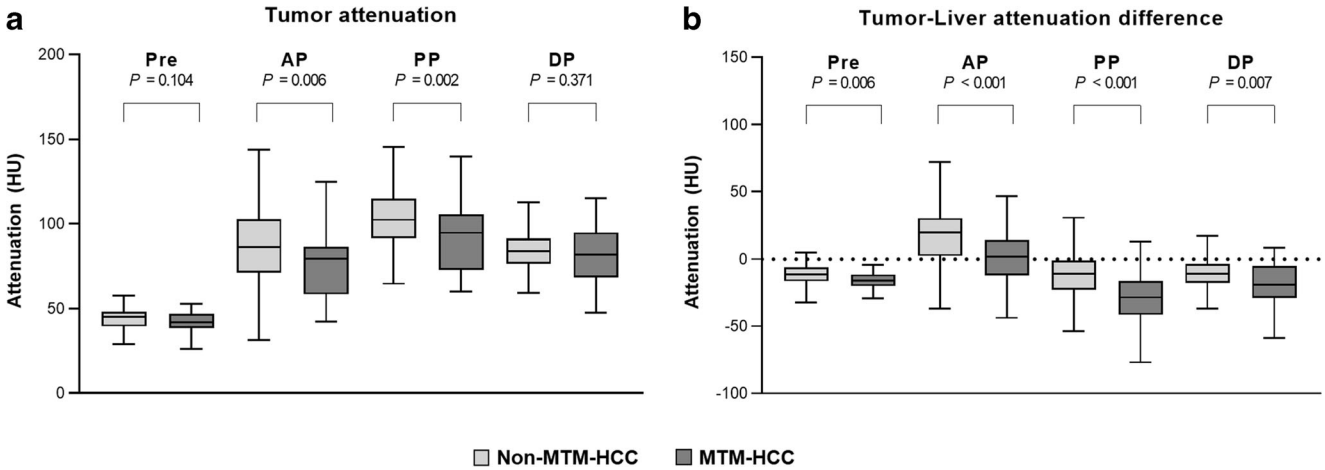

Fig. 3 Attenuation of macrotrabecular-massive hepatocellular carcinoma (MTM-HCC) versus non-MTM-HCC on computed tomography. **a** Comparison of the tumor attenuation of MTM-HCC versus non-MTM-HCC in each dynamic phase. **b** Differences in tumor and liver attenuation between MTM-HCC and non-MTM-HCC each in dynamic phase. The p values were calculated using a Mann–Whitney U test. AP, arterial phase; DP, delayed phase PP, portal phase; Pre, pre-contrast

Table 3 Prevalence of imaging findings of macrotrabecular-massive hepatocellular carcinoma (MTM-HCC) versus non-MTM-HCC

Characteristics	(1) MRI	(2) MRI, subtraction image	(3) CT	*p* value (1) vs (2)	*p* value (1) vs (3)	*p* value (2) vs (3)
MTM-HCC (*n* = 39)						
≥ 20% arterial phase hypovascular component	36 (92%)	23 (59%)	31 (80%)	< .001*	> .06	.03*
≥ 50% arterial phase hypovascular component	26 (67%)	15 (39%)	25 (64%)	< .001*	.78	.02*
Non-rim APHE	25 (64%)	32 (82%)	27 (69%)	.01*	.48	.13
LR-5	20 (59%)	26 (77%)	20 (59%)	.02*	> .99	.07
LR-M	9 (27%)	5 (15%)	8 (24%)	.03*	.32	.48
Non-MTM-HCC (*n* = 181)						
≥ 20% arterial phase hypovascular component	72 (40%)	52 (29%)	70 (39%)	< .001*	.81	.002*
≥ 50% arterial phase hypovascular component	18 (10%)	7 (4%)	26 (14%)	.002*	.13	< .001*
Non-rim APHE	163 (90%)	171 (95%)	157 (87%)	.03*	.22	.004*
LR-5	133 (79%)	139 (83%)	140 (83%)	.01*	.46	.57
LR-M	13 (8%)	9 (5%)	14 (8%)	.01*	.81	.20

*Statistically significant results from the McNemar test

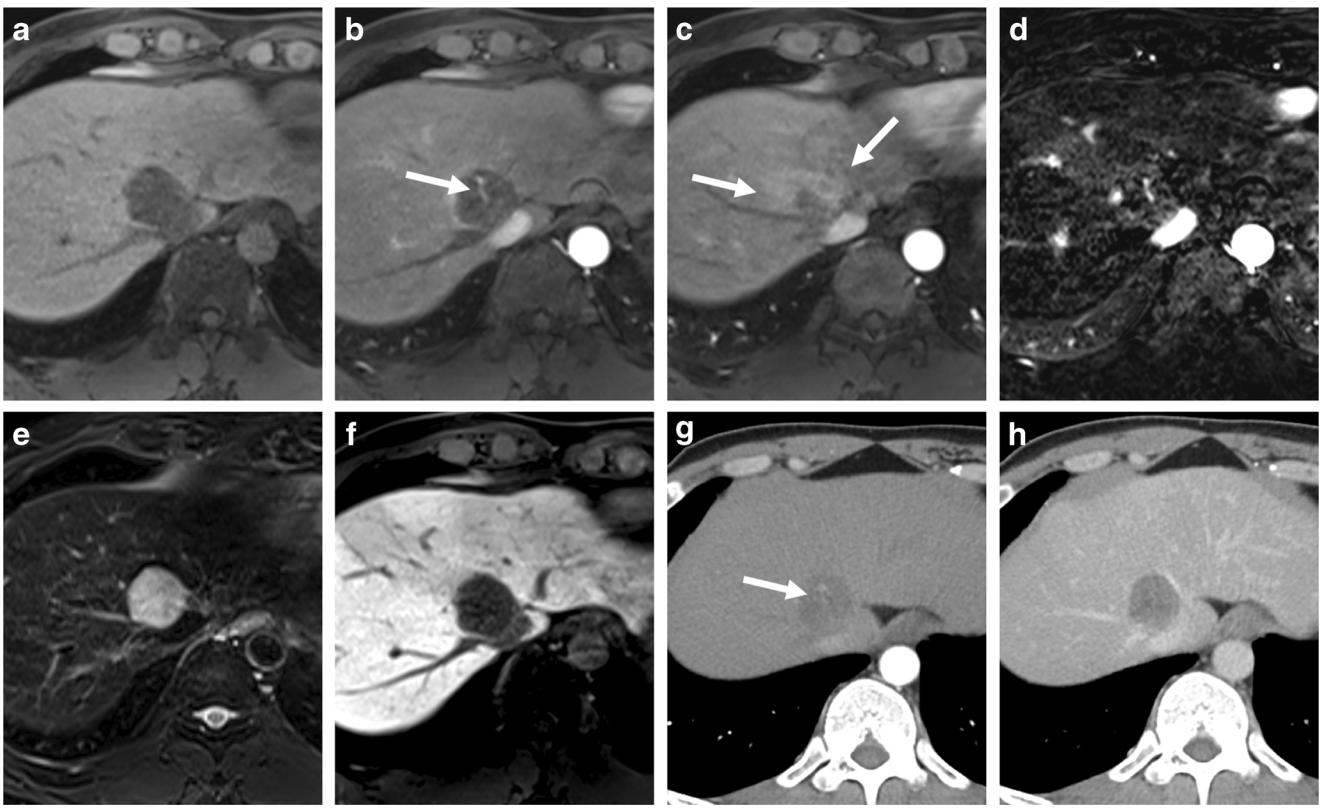

Fig. 4 A 40-year-old man with chronic hepatitis B and macrotrabecular-massive hepatocellular carcinoma (MTM-HCC). Gadoxetic acid–enhanced magnetic resonance imaging (MRI) demonstrated an approximately 3.5-cm mass in segment 8. The lesion showed absence of blood product on a T1-weighted image (**a**), diffuse (≥ 50%) hypovascular component with intratumoral artery (**b**), and arterial phase peritumoral enhancement (**c**) on arterial phase images (**b** and **c**). On an MRI arterial phase subtraction image (**d**), the lesion showed subtle non-rim arterial phase enhancement and was negative for the hypovascular component. There was no necrosis or non-smooth tumor margin on T2-weighted images (**e**) or hepatobiliary phase images (**f**), respectively. Computed tomography (CT) demonstrated ≥ 50% hypovascular component and intratumoral artery, whereas peritumoral enhancement was not well delineated in the arterial phase (**g**). Necrosis or severe ischemia was noted in the portal phase of the CT (**h**). The lesion satisfied Rhee's criteria on MRI, modified Mule's criteria on CT, and Feng's criteria on CT but did not satisfy Rhee's criteria on CT or modified Mule's criteria on MRI. After a central lobectomy, the patient survived for more than 5 years without recurrence

Table 4 Diagnostic performance of imaging features or diagnostic criteria for macrotrabecular-massive hepatocellular carcinoma (MTM-HCC)

Modality	Imaging features or diagnostic criteria	Sensitivity	Specificity	Positive-predictive value	Negative-predictive value
MRI	**Imaging features**				
	Hypovascular component (≥ 20%)	92% (36/39) [84–100%]	60% (109/181) [53–67%]	33% (36/108) [24–42%]	97% (109/112) [94–100%]
	Hypovascular component (≥ 20%), on subtraction image	59% (23/39) [44–74%]	71% (129/181) [65–78%]	31% (23/75) [20–41%]	89% (129/145) [84–94%]
	Hypovascular component (≥ 50%)	67% (26/39) [52–81%]	90% (163/181) [86–94%]	59% (26/44) [45–74%]	93% (163/176) [89–96%]
	Hypovascular component (≥ 50%), on subtraction image	38% (15/39) [23–54%]	96% (174/181) [93–99%]	68% (15/22) [49–88%]	88% (174/198) [83–92%]
	Intratumoral artery	46% (18/39) [31–62%]	83% (151/181) [78–89%]	38% (18/48) [24–51%]	88% (151/172) [83–93%]
	Arterial phase peritumoral enhancement	51% (20/39) [36–67%]	85% (154/181) [80–90%]	43% (20/47) [28–57%]	89% (154/173) [84–94%]
	Non-smooth tumor margin	72% (28/39) [58–86%]	55% (99/181) [47–62%]	25% (28/110) [17–34%]	90% (99/110) [84–96%]
	Necrosis, stippled	49% (19/39) [33–64%]	80% (144/181) [74–85%]	34% (19/56) [22–46%]	88% (144/164) [83–93%]
	Blood product in mass	31% (12/39) [16–45%]	84% (152/181) [79–89%]	29% (12/41) [15–43%]	85% (152/179) [80–90%]
	Diagnostic criteria				
	Rhee criteria[1†]	41% (16/39) [26–56%]	97% (175/181) [94–99%]	73% (16/22) [54–91%]	88% (175/198) [84–93%]
	Modified Mule's criteria[2]	33% (13/39) [19–48%] $p = .26$	97% (175/181) [94–99%] $p > .99$	68% (13/19) [48–89%] $p = .71$	87% (175/201) [82–92%] $p = .26$
	Hypovascular component (≥ 50%) on subtraction image	38% (15/39) [23–54%] $p = .78$	96% (174/181) [93–99%] $p = .74$	68% (15/22) [49–88%] $p = .67$	88% (174/198) [83–92%] $p = .76$
CT	**Imaging features**				
	Hypovascular component (≥ 20%)	79% (31/39) [67–92%]	61% (111/181) [54–68%]	31% (31/101) [22–40%]	93% (111/119) [89–98%]
	Hypovascular component (≥ 50%)	64% (25/39) [49–79%]	86% (155/181) [81–91%]	49% (25/51) [35–63%]	92% (155/169) [88–96%]
	Intratumoral artery	41% (16/39) [26–56%]	82% (148/181) [76–87%]	33% (16/49) [20–46%]	87% (148/171) [81–92%]
	Arterial phase peritumoral enhancement	26% (10/39) [12–39%]	89% (161/181) [84–94%]	33% (10/30) [16–50%]	85% (161/190) [80–90%]
	Non-smooth tumor margin	62% (24/39) [46–77%]	66% (119/181) [59–73%]	28% (24/86) [18–37%]	89% (119/134) [83–94%]
	Severe necrosis or ischemia	72% (28/39) [58–86%]	66% (119/181) [59–73%]	31% (28/90) [22–41%]	92% (119/130) [87–96%]
	Blood product in mass	5% (2/39) [0–12%]	96% (174/181) [93–99%]	22% (2/9) [0–49%]	82% (174/211) [77–88%]
	Diagnostic criteria				
	Rhee's criteria[1]	31% (12/39) [16–45%] $p = .25$	94% (170/181) [90–97%] $p = 0.10$	52% (12/23) [32–73%] $p = .06$	86% (170/197) [81–91%] $p = .18$
	Modified Mule's criteria[2]	56% (22/39) [41–72%] $p = .08$	89% (161/181) [84–94%] $p < .001$*	52% (22/42) [37–67%] $p = .02$*	90% (161/178) [86–95%] $p = .21$
	Feng's criteria[3]	72% (28/39) [58–86%] $p = .003$*	65% (117/181) [58–72%] $p < .001$*	30% (28/92) [21–40%] $p < .001$*	91% (117/128) [87–96%] $p = .16$

*Statistically significant results from the McNemar test

† Rhee's criteria in MRI were used as a reference for diagnostic performance

[1] Hypovascular component (≥ 50%) with 2 or more of intratumoral artery, arterial phase peritumoral enhancement, non-smooth tumor margin

[2] Hypovascular component (≥ 50%) with stippled necrosis on MRI, hypovascular component (≥ 50%) with necrosis/severe ischemia on CT

[3] Presence of for necrosis/severe ischemia or hemorrhage

necrosis on MRI. The sensitivity and specificity of the modified Mule criteria on MRI were 33% and 97%, respectively, and those of the ≥ 50% hypovascular component on the subtraction images were 38% and 96%, respectively. The sensitivity and specificity of these MRI criteria did not differ significantly from those of Rhee et al.

On CT, modified Mule's criteria were defined as hypovascular component (≥ 50%) with necrosis/severe ischemia, while Feng's criteria were defined as the presence of necrosis/severe ischemia or hemorrhage [12]. On CT, the sensitivity and specificity of Rhee's, modified Mule's, and Feng's criteria were 31% and 94%, 56% and 89%, and 72% and 65%, respectively. The sensitivity and specificity of Rhee's criteria on CT did not differ significantly from those on MRI (p = .25 and p = .10, respectively). The specificity was significantly lower in the modified Mule criteria on CT than in Rhee's criteria on MRI (89% vs. 97%, p < .001). For Feng's criteria on CT, the sensitivity was significantly higher (72% vs. 41%, p = .003); however, the specificity was significantly lower (65% vs. 97%, p < .001) (Fig. 5).

Prognostic significance of diagnostic criteria on CT and MRI

All of Rhee's and modified Mule's criteria on MRI (p = .001 and p = .004, respectively) and CT (p < .001 and p = .001, respectively), the ≥ 50% hypovascular component on MRI subtraction images (p = .02), and Feng's criteria on CT (p < .001) were significantly associated with a poor OS on univariate Cox analysis. All diagnostic criteria, except the ≥ 50% hypovascular component on subtraction images, were also significantly correlated with ER on univariate analysis (p = .004, p = .03, p = .01, p = .01, and p = .002, respectively) (Supplementary Table 6). Among the three diagnostic criteria on CT, Rhee's criteria demonstrated the highest hazard ratios for ER and OS (Fig. 6); therefore, Rhee's criteria on CT were used in the subsequent multivariate analysis.

In the multivariate survival analysis (Table 5), cirrhosis, high AFP, large tumor size, microvascular invasion, and satellite nodule remained independent prognostic factors for ER.

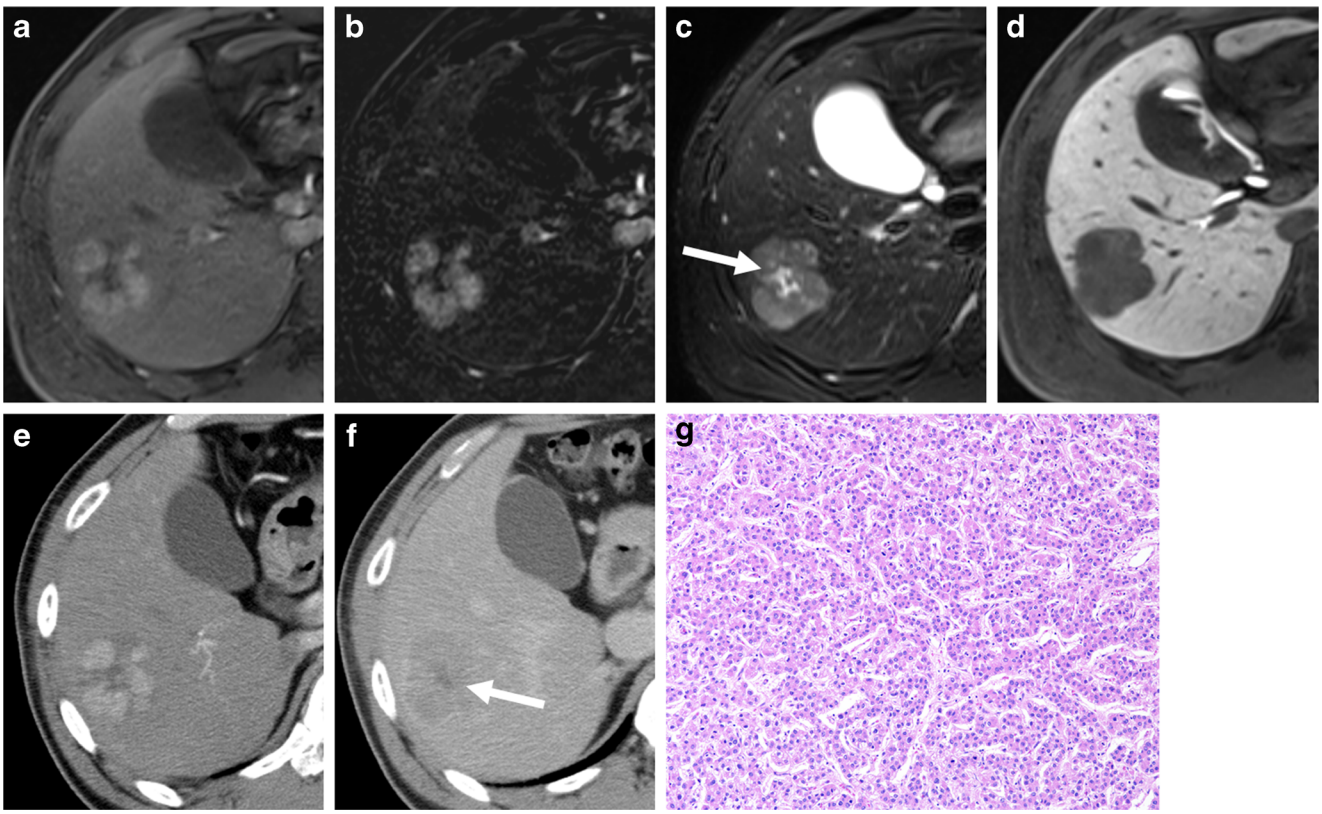

Fig. 5 A 47-year-old man with chronic B viral hepatitis and non-macrotrabecular-massive hepatocellular carcinoma (non-MTM-HCC). Gadoxetic acid–enhanced magnetic resonance imaging (MRI) demonstrating an approximately 4.1-cm HCC in the liver segment 5/6. The lesion showed non-rim arterial phase hyperenhancement and arterial hypovascular component < 50% in the arterial phase (**a**) and arterial phase subtraction image (**b**), central necrosis in T2-weighted image (**c**), and non-smooth tumor margin in hepatobiliary image (**d**). CT demonstrating non-rim arterial phase enhancement, an arterial hypovascular component < 50% in the arterial phase (**e**), and presence of necrosis or severe ischemia in the central portion of the lesion and non-smooth tumor margin in the portal phase (**f**). As the arterial hypovascular component was < 50% on MRI and CT, Rhee's and modified Mule's criteria were negative on CT and MRI, whereas Feng's criteria on CT were positive. The patient underwent a right hepatectomy, and hematoxylin-eosin staining showed a trabecular pattern less than six cells thick, suggesting non-MTM-HCC (**g**, original magnification, ×100)

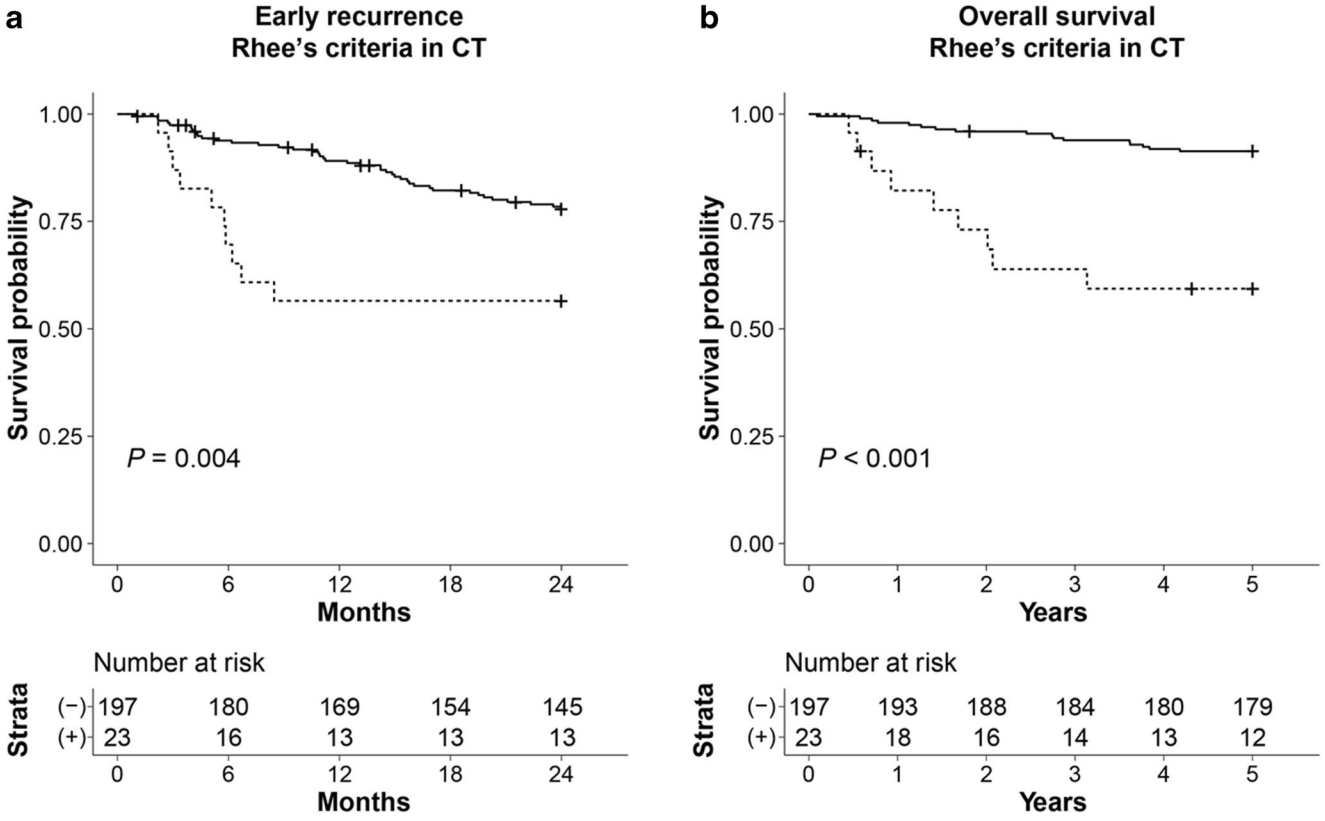

Fig. 6 Comparison of post-surgical outcomes of hepatocellular carcinoma patients according to Rhee's criteria on computed tomography (CT). Kaplan–Meier plots of early recurrence (**a**) and overall survival (**b**) according to Rhee's criteria on CT. *p* values were calculated using the log-rank test

For OS, cirrhosis, large tumor size, microvascular invasion, satellite nodule, and Rhee's criteria on CT were independent factors.

Discussion

In this study, the previously reported MRI findings of MTM-HCC showed a significant association with MTM-HCC on CT as well. Rhee's and Mule's MRI diagnostic criteria for MTM-HCC were also applicable on CT and showed a significant association with post-surgical outcomes. In particular, Rhee's criteria showed no significant difference in sensitivity and specificity between MRI and CT and were revealed as an independent prognostic factor for OS.

The most characteristic imaging finding of MTM-HCC is arterial hypovascularity. The intratumoral area showing a macrotrabecular pattern and arterial phase hypovascularity is typically seen in the inner portion of the tumor [6, 8]. Given the poor differentiation and aggressive histologic features of macrotrabecular HCC versus non-macrotrabecular HCC, it is reasonable to assume that the internal location of the hypovascular macrotrabecular area exhibits characteristics as a de-differentiated tumor component. MTM-HCC frequently exhibits rim APHE and is classified as LR-M because of the arterial hypovascularity in the inner area of the tumor [8, 16, 17]. As with MRI, CT could be used to evaluate the arterial hypovascular component, and a ≥ 20% hypovascular component demonstrated a high NPV (93%) for MTM-HCC, suggesting that HCC without a hypovascular component is highly unlikely to be MTM-HCC. In a quantitative analysis of tumor attenuation using CT, MTM-HCC showed less arterial enhancement than non-MTM-HCC as in the visual assessment using MRI or CT.

The proportion of MTM-HCC with an arterial phase hypovascular component differed by imaging modality. The MRI arterial subtraction image showed subtle hypervascularity in MTM-HCC; therefore, the arterial hypovascular component was less frequently noted than on CT or MRI. Accordingly, non-rim APHE and LR-5 were more frequently observed, whereas LR-M was less frequently observed on MRI arterial phase subtraction images than on MRI arterial phase images. Thus, MRI arterial phase subtraction images might aid in HCC diagnosis in cases of MTM-HCC. Arterial phase subtraction images are beneficial in the diagnosis of early-stage HCC [18], and our results suggest that subtraction imaging could also be beneficial for the diagnosis of a subset of advanced HCC. Interestingly, studies using gadoxetic acid–enhanced MRI found that MTM-HCC frequently (33–77%) displayed rim enhancement due to internal hypovascularity, whereas studies

Table 5 Univariate and multivariate analysis results of early recurrence and overall survival

Variables	Early recurrence				Overall survival			
	Univariate analysis		Multivariate analysis		Univariate analysis		Multivariate analysis	
	Hazard ratio (95% CI)	*p* value	Hazard ratio (95% CI)	*p* value	Hazard ratio (95% CI)	*p* value	Hazard ratio (95% CI)	*p* value
Clinical findings								
Age (≥ 60 years)	1.347 (0.7737–2.344)	.29			1.354 (0.6219–2.948)	.45		
Sex (male)	0.9231 (0.4843–1.76)	.81			1.144 (0.4314–3.034)	.79		
Etiology (hepatitis B virus)	1.192 (0.5093–2.792)	.69			1.211 (0.3635–4.032)	.76		
Cirrhosis	1.926 (1.079–3.439)	.03*	2.409 (1.3312–4.359)	.004*	2.413 (1.014–5.741)	.05*	3.012 (1.244–7.296)	.01*
Alpha-fetoprotein (≥ 400 ng/mL)	2.265 (1.243–4.128)	.01*	1.750 (0.9325–3.283)	.08	1.689 (0.678–4.206)	.26		
PIVKA-II (≥ 400 mAU/mL)	2.251 (1.28–3.96)	.005*			4.471 (2.067–9.672)	< .001*		
Tumor pathology								
Tumor size (≥ 5 cm)	2.997 (1.728–5.198)	< .001*	2.514 (1.3851–4.562)	.002*	5.258 (2.414–11.46)	< .001*	3.215 (1.398–7.394)	.01*
Differentiation (III or IV)	1.445 (0.7579–2.754)	.26			2.149 (0.9342–4.943)	.07		
Complete tumor capsule	0.5653 (0.2906–1.1)	.09			0.3994 (0.1376–1.159)	.09		
Microvascular invasion	3.375 (1.872–6.084)	< .001*	2.215 (1.1565–4.241)	.02*	10.80 (3.240–35.97)	< .001*	5.252 (1.445–19.085)	.01*
Satellite nodule	3.735 (1.594–8.755)	.002*	2.731 (1.0957–6.807)	.03*	6.865 (2.581–18.26)	< .001*	2.912 (1.050–8.076)	.04*
Radiologic finding								
Rhee's criteria on CT	2.632 (1.319–5.252)	.01*			6.046 (2.689–13.60)	< .001*	2.765 (1.169–6.544)	.02*

PIVKA-II, protein induced by vitamin K absence or antagonist-II; *CI*, confidence interval

*Statistically significant results from Cox regression analysis

using MRI contrast media other than gadoxetic acid found a lower rate (10–15%) of rim enhancement [6–8, 16, 17]. One possible explanation for this is that gadoxetic acid–enhanced MRI is less sensitive to arterial hypervascularity than other contrasts due to its low gadolinium dose [19]. It can be considered another example showing that sensitive detection of arterial hypervascularity can be helpful in the HCC diagnosis of MTM-HCC.

Necrosis may occur in HCC with a hypoxic microenvironment, including MTM-HCC [8, 20]. A positive correlation has been reported between the proportion of macrotrabecular and necrotic areas [8]. The tumor area with T2 hyperintensity and absence of enhancement indicating tumor necrosis, so-called substantial necrosis, is a proposed diagnostic criterion for MTM-HCC [7]. We further analyzed the pattern of tumor necrosis, and only stippled necrosis was significantly associated with MTM-HCC, a finding that was consistent with that of multifocal small necrosis in MTM-HCC [8]. The stippled necrosis with ≥ 50% hypovascular component on MRI (modified Mule's criteria on MRI) was highly specific (97%) for MTM-HCC. However, on CT, the criteria based on necrosis showed lower specificity (89% for modified Mule's and 65% for Feng's criteria), which might be due to limitations in the accurate evaluation of the necrotic area and pattern on CT.

Imaging findings associated with MTM-HCC on MRI are reportedly useful for diagnosis and predicting prognosis after hepatic resection [6, 7]. On CT, all composed MTM-HCC diagnostic criteria were significantly associated with a poor prognosis, and Rhee's criteria were an independent predictor of OS. Thus, particularly in clinical settings in which MRI is unfeasible, Rhee's criteria on CT could be used to predict post-surgical outcomes and aid clinical decisions.

This study had two main limitations. First, it was a retrospective single-center study. As the majority of patients at our institution underwent dynamic CT and gadoxetic acid–enhanced MRI as preoperative evaluations, those who underwent MRI with contrast media other than gadoxetic acid were excluded from the study. Second, tumor attenuation was measured with only one circular ROI rather than the entire tumor volume. Further studies using volumetric analysis with radiomics or deep learning may improve the diagnosis of MTM-HCC.

In conclusion, the MRI diagnostic criteria for MTM-HCC are applicable to CT, which showed similar diagnostic performance and prognostic significance. Arterial phase subtraction images could aid in the diagnosis of MTM-HCC by illustrating more subtle arterial hypervascularity.

Supplementary Information The online version contains supplementary material available at https://doi.org/10.1007/s00330-022-09105-7.

Funding This study was supported by a grant from the National Research Foundation of Korea (NRF) grant funded by the Korea government (MSIT) (NRF-2020R1C1C1003887).

Declarations

Guarantor The scientific guarantor of this publication is Professor Hyungjin Rhee.

Conflict of interest The authors of this manuscript declare no relationships with any companies whose products or services may be related to the subject matter of the article.

Statistics and biometry The statistical analyses were conducted under the direction of an experienced statistician (Kyunghwa Han, Ph. D.). She also participated in our manuscript as one of the authors.

Informed consent Written informed consent was waived by the Institutional Review Board.

Ethical approval Institutional Review Board approval was obtained.

Study subjects or cohorts overlap All of our 220 subjects have been previously reported in our previous study (J Hepatol. 2021 Jan; 74(1): 109–121); in fact, 88 patients (40%) and 132 patients (60%) overlapped with the training and validation sets of the previous study. The prior study dealt with MRI findings of MTM-HCC, whereas in this manuscript we investigated CT findings of MTM-HCC in comparison with MRI findings.

Methodology
- retrospective
- diagnostic or prognostic study
- performed at one institution

References

1. Boyault S, Rickman DS, de Reyniès A et al (2007) Transcriptome classification of HCC is related to gene alterations and to new therapeutic targets. Hepatology 45:42–52
2. Calderaro J, Couchy G, Imbeaud S et al (2017) Histological subtypes of hepatocellular carcinoma are related to gene mutations and molecular tumour classification. J Hepatol 67:727–738
3. Hoshida Y, Nijman SM, Kobayashi M et al (2009) Integrative transcriptome analysis reveals common molecular subclasses of human hepatocellular carcinoma. Cancer Res 69:7385–7392
4. Tan PS, Nakagawa S, Goossens N et al (2016) Clinicopathological indices to predict hepatocellular carcinoma molecular classification. Liver Int 36:108–118
5. Ziol M, Pote N, Amaddeo G et al (2018) Macrotrabecular-massive hepatocellular carcinoma: a distinctive histological subtype with clinical relevance. Hepatology 68:103–112
6. Rhee H, Cho ES, Nahm JH et al (2021) Gadoxetic acid-enhanced MRI of macrotrabecular-massive hepatocellular carcinoma and its prognostic implications. J Hepatol 74:109–121
7. Mule S, Galletto Pregliasco A, Tenenhaus A et al (2020) Multiphase liver MRI for identifying the macrotrabecular-massive subtype of hepatocellular carcinoma. Radiology 295:562–571
8. Rhee H, An C, Kim HY, Yoo JE, Park YN, Kim MJ (2019) Hepatocellular carcinoma with irregular rim-like arterial phase

hyperenhancement: more aggressive pathologic features. Liver Cancer 8:24–40
9. Calderaro J, Meunier L, Nguyen CT et al (2019) ESM1 as a marker of macrotrabecular-massive hepatocellular carcinoma. Clin Cancer Res 25:5859–5865
10. An C, Park MS, Kim D et al (2013) Added value of subtraction imaging in detecting arterial enhancement in small (<3 cm) hepatic nodules on dynamic contrast-enhanced MRI in patients at high risk of hepatocellular carcinoma. Eur Radiol 23:924–930
11. Roberts LR, Sirlin CB, Zaiem F et al (2018) Imaging for the diagnosis of hepatocellular carcinoma: a systematic review and meta-analysis. Hepatology 67:401–421
12. Feng Z, Li H, Zhao H et al (2021) Preoperative CT for characterization of aggressive macrotrabecular-massive subtype and vessels that encapsulate tumor clusters pattern in hepatocellular carcinoma. Radiology 300:219–229
13. Segal E, Sirlin CB, Ooi C et al (2007) Decoding global gene expression programs in liver cancer by noninvasive imaging. Nat Biotechnol 25:675–680
14. An C, Kim DW, Park YN, Chung YE, Rhee H, Kim MJ (2015) Single hepatocellular carcinoma: preoperative MR imaging to predict early recurrence after curative resection. Radiology 276:433–443
15. American College of Radiology, Liver Imaging Reporting and Data System version 2018, https://www.acr.org/Clinical-Resources/Reporting-and-Data-Systems/LI-RADS/CT-MRI-LI-RADS-v2018.
16. Cannella R, Dioguardi Burgio M, Beaufrère A et al (2021) Imaging features of histological subtypes of hepatocellular carcinoma: implication for LI-RADS. JHEP Reports. https://doi.org/10.1016/j.jhepr.2021.100380:100380
17. Kang HJ, Kim H, Lee DH et al (2021) Gadoxetate-enhanced MRI features of proliferative hepatocellular carcinoma are prognostic after surgery. Radiology. https://doi.org/10.1148/radiol.2021204352:204352
18. Kim DH, Choi SH, Byun JH et al (2019) Arterial subtraction images of gadoxetate-enhanced MRI improve diagnosis of early-stage hepatocellular carcinoma. J Hepatol 71:534–542
19. Min JH, Kim JM, Kim YK et al (2018) Prospective intraindividual comparison of magnetic resonance imaging with gadoxetic acid and extracellular contrast for diagnosis of hepatocellular carcinomas using the liver imaging reporting and data system. Hepatology 68:2254–2266
20. Rhee H, Nahm JH, Kim H et al (2016) Poor outcome of hepatocellular carcinoma with stemness marker under hypoxia: resistance to transarterial chemoembolization. Mod Pathol 29:1038–1049